

Article

A Seedbed Clearing and Shaping Device for Dry Direct-Seeded Rice

Hui Li ¹, Longyu Fang ², Pingping Yuan ¹, Wei Lu ¹ and Wenwu Yang ^{2,3,4,*}

¹ Hunan Academy of Agricultural Sciences, Changsha 410125, China

² Key Laboratory of Key Technology on Agricultural Machine and Equipment, Ministry of Education, South China Agricultural University, Guangzhou 510642, China

³ Huangpu Innovation Research Institute, South China Agricultural University, Guangzhou 510725, China

⁴ Maoming Branch, Guangdong Laboratory for Modern Agriculture, Maoming 525000, China

* Correspondence: yangwenwu@scau.edu.cn

Abstract: The soil in some areas of northern China is heavy owing to the presence of clay and stones, which significantly affects the normal operation of a planter as well as the growth of rice. In this regard, this study proposes a seedbed clearing and shaping device for dry direct-seeded rice, which can be used to remove stones in the seeding area, break soil blocks, for soil leveling, and groove forming. The overall structure and roller of the proposed device was developed based on theoretical calculations, discrete element modeling (DEM) simulations, and field tests. The soil-mixing tooth was distributed on the roller based on the double-helix rule, and the two sides of the helix were configured according to the right-hand and left-hand. Subsequently, DEM was used to develop a 3³ box-bench design. According to the agronomic requirements and operating speed ratio, the forward speed was set to 0.5 m/s. Furthermore, the optimization parameters combination of the device obtained by simulation experiments was: forward speed 0.5 m/s, soil depth 61 mm, and rotation speed 110 r/min, which obtained a stone removal rate of 85.65%, stone removal efficiency of 35.47 pieces/m, operating resistance of 719.23 N, and torque of 174.89 Nm. The field verification test results indicated that the stone removal rate was 77.23% under the optimization parameters combination, and the mean relative error of the simulated experiments value was 8.42%, which showed that the performance of the proposed device functioned stably and reliably, thereby providing a high-quality seedbed for sowing and rice growth. The developed device represents a useful solution for the seedbed clearing and shaping.

Keywords: seedbed clearing and shaping; stone removal rate; seeding furrow; dry direct-seeded rice; discrete element modeling



Citation: Li, H.; Fang, L.; Yuan, P.; Lu, W.; Yang, W. A Seedbed Clearing and Shaping Device for Dry Direct-Seeded Rice. *Agriculture* **2022**, *12*, 1740. <https://doi.org/10.3390/agriculture12101740>

Academic Editors: Mustafa Ucgul and Chung-Liang Chang

Received: 10 September 2022

Accepted: 20 October 2022

Published: 21 October 2022

Publisher's Note: MDPI stays neutral with regard to jurisdictional claims in published maps and institutional affiliations.



Copyright: © 2022 by the authors. Licensee MDPI, Basel, Switzerland. This article is an open access article distributed under the terms and conditions of the Creative Commons Attribution (CC BY) license (<https://creativecommons.org/licenses/by/4.0/>).

1. Introduction

Rice is considered the main food crop, with over 50% of the world's population consuming rice [1]. Rice transplanting is a traditional rice cultivation method used in Asia with a long history, which can shorten the growth period of rice and ensure the number of seedlings in the field is conducive to a high and stable yield [2]. Rice transplanting is a highly labor-intensive and water-intensive method of cultivation [3–5]. However, there is shortage of labor resources owing to the development of the economy and society, and labor costs have gradually increased. As a result, agriculture has become less profitable [6,7]. Dry direct-seeded rice is an important choice for solving the shortage of labor and water resources [8,9]. Singh et al. [10] reported that compared to rice transplanting, direct-seeded rice could save 56% labor, 73% mechanical work, and 25% irrigation water. Therefore, direct-seeded rice technology could increase farmers' income and save natural resources. Furthermore, because this technology directly sows seeds into the field without seedling raising or transplanting, the process is simple and easy to operate [11,12]. Previous studies

show that the yield of dry direct-seeded rice can be compared to that of the rice transplanting method [13–15]. However, because dry direct-seeded rice is more susceptible to climate and weeds, field management is an important factor that affects the yield [16–18]. To solve the problems of direct-seeded rice, foreign and domestic experts have carried out research on dry direct-seeded rice with film mulching [19,20].

The quality of the seedbed affects the sowing quality and growth of the rice [21,22], and dry direct-seeded rice with film mulching requires soft, fine, and smooth seedbed soil. However, in some areas of northern China, the soil is heavy with clay and stones, which significantly affects the normal operation of the planter as well as the growth of the rice. Moreover, owing to the hardness of the stone, when the planter, plastic film, and stone interact, the plastic film is scraped and broken, which significantly affects the performance of the plastic film.

In view of the problems of dry direct-seeded rice with film mulching in northern China, most research adopts high-power tractors that support stone-picking machines and tools for deep scavenging, or uses a sieve device to wash the soil. However, the above devices consume a large amount of power during operation, resulting in soil layer chaos and soil structure destruction. These devices focus on the number of stones picked up, and seldom care about how many stones are present in the topsoil, because disturbances in the deep soil can turn the bottom stones over to the surface of the soil, which does not solve the problems of stones in the seedbed. Although several studies have been conducted on the stone-removal equipment of the minimum soil layer, namely, the seeding area, in seedbeds in northern China, there are no relevant reports on the effect of the machines' working parameters on the operation effect and performance.

Therefore, this study developed a seedbed clearing and shaping device for dry direct-seeded rice aiming at the complex structure, high power, and large soil disturbance of the existing equipment. The proposed device can be used to remove stones in the seeding area, break soil blocks, and for soil leveling and groove forming, which works on the top soil without disturbing the deep soil to clean the sowing layer of the soil. Furthermore, we carried out the optimal design of the key structural components, and simulation experiments and field tests were conducted to analyze its operation performance and working effect to obtain the optimal combination of parameters of the device. The proposed device provides new technology and equipment for the development of precision agriculture.

2. Structure and Working Principles of the Proposed Device

2.1. Machine Structure

Figure 1 shows the overall structure of the proposed seedbed clearing and shaping device for dry direct-seeded rice. The device comprises a frame, belt-driving system, gear reducer, drip irrigation belt, guiding tube of the drip irrigation belt, protective board, soil-mixing tooth, roller, groove-pressing roller, plastic film, and a depth-limiting wheel, along with other components.

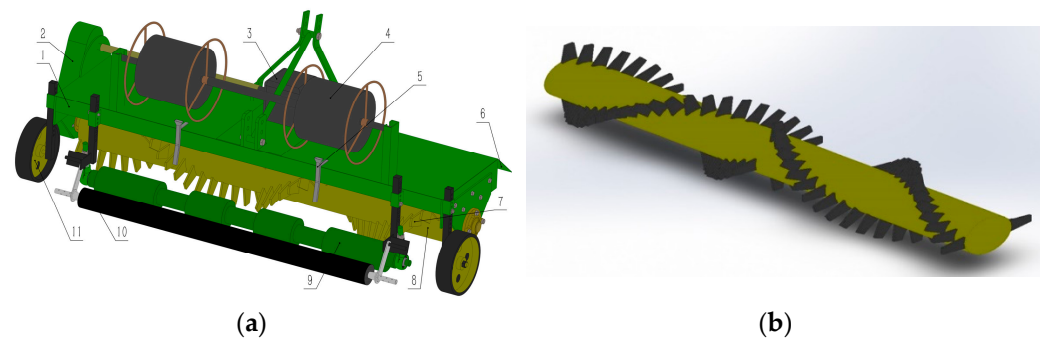


Figure 1. Structural diagram of the proposed seedbed clearing and shaping device for dry direct-seeded rice: (a) mechanical structure of the device: 1. frame; 2. belt-driving system; 3. gear reducer; 4. drip irrigation belt; 5. guiding tube of the drip irrigation belt; 6. protective board; 7. soil-mixing tooth; 8. roller; 9. groove-pressing roller; 10. plastic film; and 11. depth-limiting wheel. (b) Roller with soil-mixing teeth.

2.2. Working Principle

The proposed device for dry direct-seeded rice is connected to a tractor using the trifilar suspension system, and parallel four-bar linkages are connected to sowing devices; each set of sowing devices can float freely depending on the terrain. Figure 2 shows the working principle of the proposed device. According to the agronomic requirements of rice cultivation, the parameters of the corresponding work module, such as the height of the groove-pressing roller and depth-limiting wheel, should be adjusted prior to field operation.

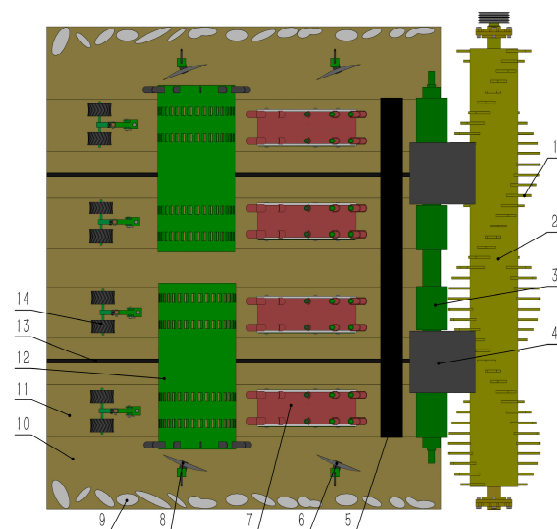


Figure 2. Working principle of the seedbed clearing and shaping device for dry direct-seeded rice. It comprises: 1. soil-mixing tooth; 2. roller; 3. groove-pressing roller; 4. drip irrigation belt; 5. plastic film; 6. soil-covering disk-1; 7. sowing device; 8. soil-covering disk-2; 9. stone and caking soil; 10. ridge; 11. seeding furrow; 12. soil-covering roller; 13. drip irrigation belt; and 14. soil-suppression device.

The power output shaft of the tractor provides an adequate running drive for the seedbed clearing and shaping device. The stones and soil blocks in the topsoil are thrown upward and forward using the rotary roller, and a part of the soil block is broken by collision with the soil-mixing tooth. Stones and soil blocks are conveyed to both sides of the device by the soil-mixing tooth with a spiral pattern distribution on the roller; the loose earth is not transported. The clearing operations are directed only at the sowing soil layer to reduce the disturbance to the deep soil and stones. When the groove-pressing roller rotates forward, it fills the shallow gullies and presses out the seeding furrow with a depth

of 30–40 mm, thereby forming four regular seeding furrows and five ridges. Then, the seeds are sown in the corresponding seeding furrow, so the device provides a high-quality seedbed for the seeding operations and growth of rice.

The parameters of the proposed device have a direct effect on the quality of the seedbeds, and hence, are a key component of the planter for achieving the process of seedbed stone and soil block clearing and seeding furrow shaping. Therefore, according to the agronomic requirements of rice cultivation in the area of northern China, the sowing depth should be between 15 and 25 mm; that is, the stones and soil blocks should be removed from the 50 mm soil layer to form a clean seeding area, and the working depth of the soil-mixing tooth can be adjusted between 0 and 100 mm by controlling the height of the depth-limiting wheel. The width of the seeding furrow is determined to 200 mm based on the agronomy requirements (large and small row spacings are 250 mm and 120 mm, respectively) and combining the actual size of the sowing device to improve the utilization rate of natural rainfall, the depth of the seeding furrow is selected as 35 mm depending on the results of the preliminary experiments.

2.3. Structural Design of Critical Component

The soil-mixing tooth and roller are the key components of the device, since they directly affect the effects of seedbed clearing and shaping. The device adopts a harrow-type mechanism to pick up stones. The soil-mixing teeth are distributed on the roller according to the double-helix rule, and both sides of the helix are configured according to the right and left hands, respectively. The stones and soil blocks move to the two sides for the clearing of the seedbed.

2.3.1. Kinematic Equation of the Endpoint of the Soil-Mixing Tooth

A Cartesian coordinate system is established, and the center of the roller is considered the original point O , whereas the forward direction and the direction perpendicular to the ground of the tractor is the positive direction of the X - and Y -axes, respectively. After time t , the tractor drives the roller from the original point O to O_1 . The endpoint of the soil-mixing tooth was rotated by ωt degrees from point A to point A_1 , whose coordinates are $A_1(x, y)$. Figure 3 shows the motion process. The parametric equation of the endpoint $A_1(x, y)$ of the soil-mixing tooth is the equation with time t as the variable, as shown in Equation (1). The trajectory of the endpoint of the soil-mixing tooth is an inverted trochoid formed by combining horizontal linear and circular motions.

$$\begin{cases} x = V_m t + R_m \cos(\omega t) \\ y = R_m \sin(\omega t) \end{cases} \quad (1)$$

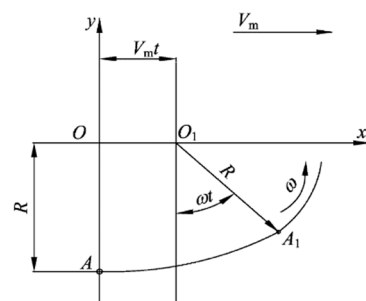


Figure 3. Motion model of the endpoint of the soil-mixing tooth.

V_m —speed of tractor, m/s;

R_m —radius of turn at the endpoint of the soil-mixing tooth, m;

ω —rotational angular velocity of the soil-mixing tooth, rad/s;

t —time, s.

2.3.2. Operating Speed Ratio

Operating speed ratio λ is the ratio of the line speed of the endpoint of the soil-mixing tooth and the speed of the tractor, which is crucial for the normal operation of the device:

$$\lambda = \frac{R_m \omega}{V_m} \quad (2)$$

Substituting Equation (2) into Equation (1), we get:

$$\begin{cases} x = R_m \left(\frac{\omega t}{\lambda} + \cos(\omega t) \right) \\ y = R_m \sin(\omega t) \end{cases} \quad (3)$$

According to Equation (3), if R_m , ω and λ are known, the coordinates of the endpoint of the soil-mixing tooth can be calculated to obtain the motion trajectory. Figure 4 shows $R_m = 210\text{mm}$, $\omega = 3.2\pi$, and the motion trajectory of the endpoint of the soil-mixing tooth when the operation speed ratio $\lambda > 1$, $\lambda = 1$ and $\lambda < 1$. As seen from the figure, when $\lambda \leq 1$, the motion trajectory is a short trochoid without overlap, that is, there is a soil pushing and leakage area, and the device cannot work normally. When $\lambda > 1$, the motion trajectory is a trochoid. Therefore, $\lambda > 1$ is an important condition for the normal operation of the device.

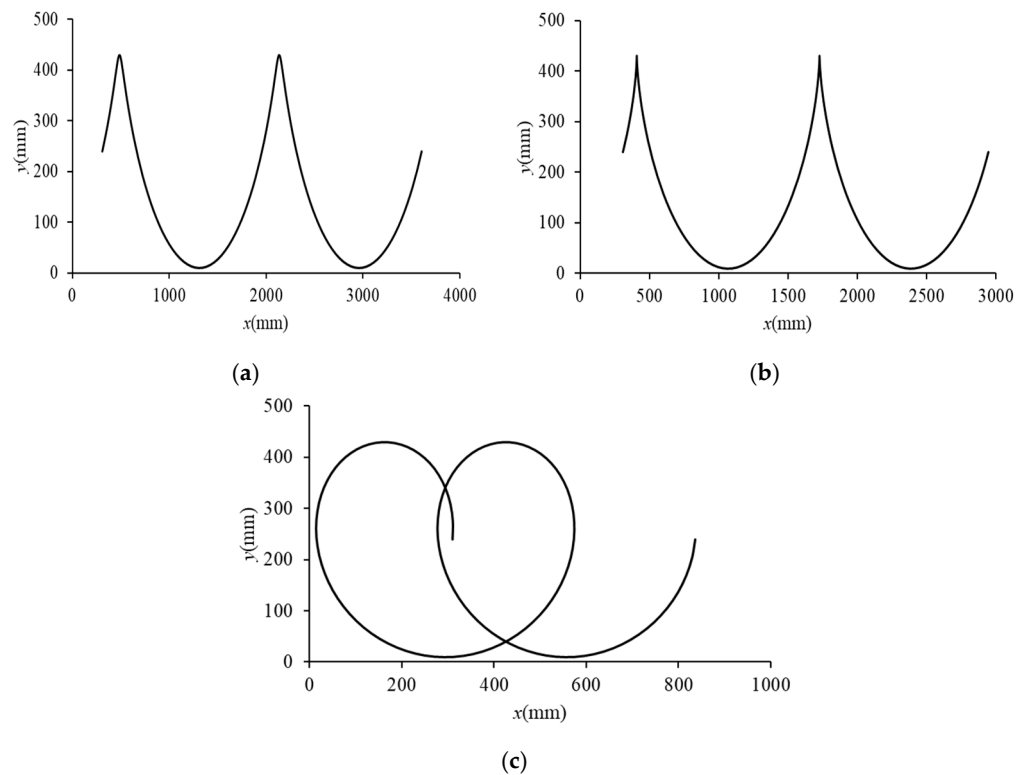


Figure 4. Motion trajectory of the endpoint of the soil-mixing tooth: (a) $\lambda < 1$; (b) $\lambda = 1$; (c) $\lambda > 1$.

2.3.3. Speed of the Endpoint of the Soil-Mixing Tooth

Equation (3) expresses the position of the endpoint of soil-mixing tooth at any time. The motion trajectory changes with the speed of tractor V_m , the radius of turn R_m , and the rotational angular velocity ω . We take the derivative of Equation (3) with respect to time to obtain the partial velocities of the endpoint of the soil-mixing tooth in the x and y directions:

$$\begin{cases} V_x = \frac{dx}{dt} = R_m \left(\frac{\omega}{\lambda} - \omega \sin \omega t \right) \\ V_y = \frac{dy}{dt} = \omega \cos \omega t \end{cases} \quad (4)$$

Then, the instantaneous velocity V of the endpoint of the soil-mixing tooth is:

$$V = \sqrt{V_x^2 + V_y^2} = V_m \sqrt{1 - 2\lambda \sin \omega t + \lambda^2} \quad (5)$$

3. Materials and Methods

Discrete element modeling (DEM) was adopted to carry out the simulation experiments of the seedbed clearing and shaping to improve the stone removal rate of the 50 mm soil layer and reduce the operating resistance to decrease the power consumption of the tractor, as well as to avoid manual repeatability experiments and reduce the intensity of labor. Accordingly, scientific and reliable working parameters of the device can be obtained.

3.1. Simulation Model Creation and Parameter Setting

The interaction between the dispersed particles and the soil operation machine involves complex mechanical problems, making the study of soil-touching parts difficult. Furthermore, there is currently no precise mathematical model for predicting the interactions of different operating environments. At present, the design and optimization of the soil-touching device mostly adopts the method of virtual simulation, among which DEM is an advanced and mature numerical simulation method for the discontinuous medium problem. In recent years, DEM has been widely applied in agricultural engineering, which mainly focuses on agricultural materials science and the application and research of the interaction between the soil and soil-touching parts. Therefore, this study adopted the EDEM 2018 software to simulate the seedbed clearing and shaping process and conduct the simulation experiments. The purpose of the DEM simulation experiments is to establish the regression equations of stone removal rate (y_1), stone removal efficiency (y_2), operating resistance (y_3), and torque (y_4), to understand the operation law and mechanism of the device, and to obtain the optimal combination of operation parameters to achieve high efficiency and energy-saving operations.

Figure 5a shows the simplified simulation model of the seedbed clearing and shaping device imported into the software preprocessing module.

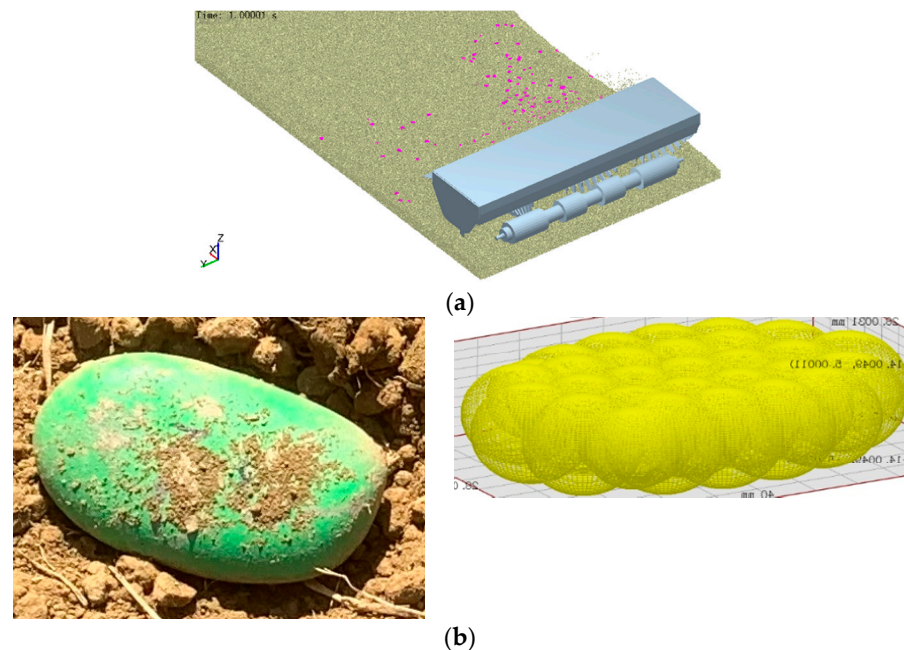


Figure 5. Simulation model: (a) simplified model of the device; (b) stone and stone particle model.

Multi-spherical polymerization was selected based on the characteristics of the stone shapes. A total of 35 sphere models were connected to construct the stone particle models (as shown in Figure 5b). The distribution of soil particle size was statistically analyzed using

a size-grading sieve. The soil particles were divided into four grades, and nearly 50% of the soil particles were in the range of 1–2.36 mm. Combined with the computer performance and the actual situation of the simulation, the soil particle model considered spheres with a diameter of 2 mm, and the diameter was generated by the normal random distribution method to accord with the realistic irregularity of actual soil. The cutting-ring method was used to measure the soil density, which was repeated five times, and the average soil density was $1914 \text{ kg}\cdot\text{m}^{-3}$. Other soil parameters were determined based on the available parameters and relevant literature [23–25]. The soil particle model was calibrated with the angle of repose as the response value, and the relative error between the actual and the model was 2.89%. The Hertz–Mindlin (no-slip) contact model included in the EDEM 2018 software was used for the simulation analysis, and with reference to the relevant literature [26–28]. Table 1 summarizes the simulation experiment parameters, which were obtained through experimental measurement and references [29,30], and calibrated by EDEM. Based on the actual number of stones in the 50 mm soil layer, 240 stone particles were generated, the size of the soil tank was $4500 \times 2400 \times 150 \text{ mm}$ (length \times width \times height), and the fixed time step was set to 20% of the Rayleigh time step ($8.86 \times 10^{-7} \text{ s}$).

Table 1. Simulation experiment parameters.

Materials	Parameters	Value
Stone	Density ($\text{kg}\cdot\text{m}^{-3}$)	2470
	Poisson ratio	0.22
	Shear modulus (Mpa)	4500
Soil	Density ($\text{kg}\cdot\text{m}^{-3}$)	1914
	Poisson ratio	0.38
	Shear modulus (Mpa)	1
Steel	Density ($\text{kg}\cdot\text{m}^{-3}$)	7850
	Poisson ratio	0.3
	Shear modulus (Mpa)	79,000
Stone–Stone	Elastic restitution coefficient	0.58
	Static friction coefficient	0.55
	Rolling friction coefficient	0.05
Soil–Soil	Elastic restitution coefficient	0.11
	Static friction coefficient	0.6
	Rolling friction coefficient	0.4
Stone–Steel	Elastic restitution coefficient	0.54
	Static friction coefficient	0.5
	Rolling friction coefficient	0.05
Soil–Steel	Elastic restitution coefficient	0.12
	Static friction coefficient	0.3
	Rolling friction coefficient	0.05
Stone–Soil	Elastic restitution coefficient	0.21
	Static friction coefficient	0.4
	Rolling friction coefficient	0.15

3.2. Scheme and Method of Simulation Experiment

According to the previous analysis and preliminary experimental results, the main operating parameters that affect the rice seedbed clearing and shaping, and the device working performance, namely, the forward speed V , soil depth H , and rotation speed n , were selected as the experimental factors. Furthermore, the stone removal rate (y_1), stone removal efficiency (y_2), operating resistance (y_3), and torque (y_4) were analyzed.

The simulation experiment using the box–bench design with three factors and three levels was conducted to evaluate the operating performance of the proposed device. Furthermore, preliminary combined factor experiments were conducted to determine the range

of the experimental factors; the forward speed of the tractor is 0.4–0.8 m/s, soil depth is 40–80 mm, and the rotation speed is 70–130 r/min. Table 2 summarizes the code value of the simulation experimental factors, and Table 3 summarizes the 20 groups of simulation experiment schemes.

Table 2. Code of simulation experiment factors.

Code Value	Forward Speed V ($m \cdot s^{-1}$)	Soil Depth H (mm)	Rotation Speed n (r/min)
1.682	0.9364	93.636	150.45
1	0.8	80	130
0	0.6	60	100
−1	0.4	40	70
−1.682	0.2636	26.364	49.55

Table 3. Simulation experiment scheme and results.

No	Forward Speed V ($m \cdot s^{-1}$)	Soil Depth H (mm)	Rotation Speed n (r/min)	Stone Removal Rate y_1 (%)	Stone Removal Efficiency y_2 (pieces/m)	Operating Resistance y_3 (N)	Torque y_4 (Nm)
1	0	0	0	91.833	34	763.582	173.014
2	1	−1	−1	71.250	18	483.361	92.290
3	0	0	−1.682	85.896	44	802.878	137.276
4	−1	1	1	87.083	40	655.782	183.634
5	0	0	0	88.667	34	773.245	177.796
6	0	−1.682	0	72.042	8	308.313	63.606
7	−1	1	−1	92.229	48	872.667	197.637
8	0	0	0	91.042	35	783.080	181.173
9	0	0	0	90.646	31	790.377	184.534
10	1	1	1	94.604	35	1163.770	284.721
11	1	1	−1	91.833	41	1354.200	260.389
12	1	−1	1	86.688	9	587.393	123.762
13	0	1.682	0	94.208	34	1171.120	291.075
14	−1	−1	−1	83.521	32	363.198	74.709
15	0	0	0	88.667	35	794.315	182.652
16	0	0	1.682	87.875	28	734.938	189.452
17	−1	−1	1	83.125	12	408.024	94.846
18	1.682	0	0	90.646	33	985.338	202.627
19	0	0	0	88.667	31	780.920	179.834
20	−1.682	0	0	83.521	43	432.149	114.310

During the experiments, when the work of the device was stable, the post-processing module of the EDEM 2018 software was used to establish the upper and lower two-layer grids with soil depths between 0–50 mm and 50–100 mm, respectively, in the region of determination. The index y_1 is the ratio between the number of stones removed to both sides of the device and the total amount of stones during the simulation process. The index y_2 is the number of stones removed to both sides of the device among the unit length during the normal operation section. The index y_3 and y_4 can be obtained directly by using the post-processing module of the EDEM 2018 software.

3.3. Data Analysis

The mechanical properties of the proposed seedbed clearing device was evaluated through the simulation experiment and field tests. The data processing and analysis were performed using Microsoft Excel and Design Expert software.

4. Results and Discussion

4.1. Variance Analysis and Discussion

Table 3 summarizes the results of the simulation experiments. The simulation data were then used to establish the regression equations, and variance analysis was carried out to verify the validity of the regression equations and significance of the items of the regression equations. Simultaneously, the secondary optimization of the regression equation was carried out to eliminate insignificant items. The optimized regression equations are shown in Equations (6)–(9), which were subjected to ANOVA again, as shown in Tables 4–7, respectively.

$$y_1 = 72.311 - 75.359V + 0.974H - 0.04n + 0.495VH + 0.495VN - 0.004Hn - 0.005H^2 \quad (6)$$

$$y_2 = 3.135 - 1.53V + 0.1732H - 0.0459n + 0.0005Hn - 0.0014H^2 \quad (7)$$

$$y_3 = -696.2 + 274.7925V + 16.3075H + 6.0424n + 21.5622VH - 0.1159VN - 629.9684V^2 - 0.0356H^2 \quad (8)$$

$$y_4 = -133.7567 + 40.8698V + 2.0403H + 1.6016n + 3.667VH + 1.0348VN - 0.0086Hn - 194.1504V^2 - 0.0067n^2 \quad (9)$$

Table 4. ANOVA of the regression equation of stone removal rate.

Source	Sum Of Squares	df	Mean Square	F-Value	p-Value
Model	679.78	7	97.11	17.23	<0.0001 *
V	7.92	1	7.92	1.4	0.2588
H	450.6	1	450.6	79.94	<0.0001 *
n	18.73	1	18.73	3.32	0.0933
VH	31.34	1	31.34	5.56	0.0362 *
Vn	70.51	1	70.51	12.51	0.0041 *
Hn	37.92	1	37.92	6.73	0.0235 *
H ²	62.76	1	62.76	11.13	0.0059 *
Residual	67.64	12	5.64		
Lack of Fit	57.48	7	8.21	4.04	0.0717
Pure Error	10.16	5	2.03		
Cor Total	747.41	19			

$R^2 = 0.9095$; $R^2_{adj} = 0.8567$; $CV = 2.72\%$; adequate precision = 15.9099. Note: * shows the term is significant ($p < 0.05$).

Table 5. ANOVA of the regression equation of stone removal efficiency.

Source	Sum of Squares	df	Mean Square	F-Value	p-Value
Model	24.93	5	4.99	63.75	<0.0001 *
V	1.28	1	1.28	16.35	0.0012 *
H	14.89	1	14.89	190.35	<0.0001 *
n	3.37	1	3.37	43.07	<0.0001 *
Hn	0.6872	1	0.6872	8.79	0.0103 *
H ²	4.71	1	4.71	60.18	<0.0001 *
Residual	1.09	14	0.0782		
Lack of fit	0.9629	9	0.107	4.06	0.0687
Pure error	0.1319	5	0.0264		
Cor total	26.02	19			

$R^2 = 0.9579$; $R^2_{adj} = 0.9429$; $CV = 5.11\%$; adequate precision = 28.3661. Note: * shows the term is significant ($p < 0.05$).

Table 6. ANOVA of the regression equation of the operating resistance.

Source	Sum Of Squares	df	Mean Square	F-Value	P-Value
Model	1459000	7	208400	678.96	<0.0001 *
<i>V</i>	360700	1	360700	1175.06	<0.0001 *
<i>H</i>	978500	1	978500	3187.73	<0.0001 *
<i>n</i>	10172.1	1	10172.1	33.14	<0.0001 *
<i>VH</i>	59510.6	1	59510.6	193.88	<0.0001 *
<i>Hn</i>	38666.1	1	38666.1	125.97	<0.0001 *
<i>V</i> ²	9241.95	1	9241.95	30.11	<0.0001 *
<i>H</i> ²	2954.75	1	2954.75	9.63	0.0091 *
Residual	3683.35	12	306.95		
Lack of fit	3050.32	7	435.76	3.44	0.0962
Pure error	633.04	5	126.61		
Cor total	1463000	19			

$R^2 = 0.9948$; $R^2_{adj} = 0.9910$; $CV = 3.57\%$; adequate precision = 56.0155. Note: * shows the term is significant ($p < 0.05$).

Table 7. ANOVA of the regression equation of torque.

Source	Sum of Squares	df	Mean Square	F-Value	P-Value
Model	77034.4	8	9629.29	262.91	< 0.0001 *
<i>V</i>	9430.16	1	9430.16	257.47	< 0.0001 *
<i>H</i>	62425.7	1	62425.7	1704.41	< 0.0001 *
<i>n</i>	1640.63	1	1640.63	44.79	< 0.0001 *
<i>VH</i>	1721.18	1	1721.18	46.99	< 0.0001 *
<i>Vn</i>	308.39	1	308.39	8.42	0.0144 *
<i>Hn</i>	213	1	213	5.82	0.0345 *
<i>V</i> ²	877.81	1	877.81	23.97	0.0005 *
<i>n</i> ²	530.14	1	530.14	14.47	0.0029 *
Residual	402.89	11	36.63		
Lack of fit	320.39	6	53.4	3.24	0.1092
Pure error	82.49	5	16.5		
Cor total	77437.2	19			

$R^2 = 0.9948$; $R^2_{adj} = 0.9910$; $CV = 3.57\%$; adequate precision = 56.0155. Note: * shows the term is significant ($p < 0.05$).

The variance analysis of the regression equations of the stone removal rate (y_1), stone removal efficiency (y_2), operating resistance (y_3), and torque (y_4) showed that the regression equations were significant without the lack of fit, thereby indicating that the regression equations were effective and can be used to predict the response value. The significance ordering of the forward speed V , soil depth H , and rotation speed n on the stone removal rate (y_1), stone removal efficiency (y_2), operating resistance (y_3), and torque (y_4) were soil depth $H >$ forward speed $V >$ rotation speed n , soil depth $H >$ rotation speed $n >$ forward speed V , soil depth $H >$ forward speed $V >$ rotation speed n , and soil depth $H >$ forward speed $V >$ rotation speed n , respectively.

4.2. Interactive Analysis and Discussion

The stone removal rate (y_1), stone removal efficiency (y_2), operating resistance (y_3), and torque (y_4) were not only affected by the forward speed V , soil depth H , rotation speed n , but also by the interactions between the factors, considering that partial interactions significantly affect the response value. Based on the analysis of variance of the regression equations, the response surfaces were analyzed and discussed.

4.2.1. Stone Removal Rate

The soil depth has a significant effect on the stone removal rate. Although the forward speed and rotation speed affect the stone removal rate, it is not significant. However, there were significant interaction effects among the three factors, and the quadratic term of the

soil depth significantly affects the stone removal rate. As shown in Figure 6a, the effect of soil depth on the stone removal rate is significantly stronger than the forward speed; when the soil depth is small, the stone removal rate changes slightly or decreases as the forward speed increases. When the soil depth is approximately 60 mm, the stone removal rate increases as the forward speed increases, and the increasing trend increases. The increasing soil depth increases the stone removal rate, whereas the increasing trend of the stone removal rate increases with the increasing forward speed. As shown in Figure 6b, when the forward speed is small, the stone removal rate changes slightly as the rotation speed increases. When the forward speed is large, the stone removal rate gradually increases as the rotation speed increases; the effect of the forward speed on the change of the stone removal rate is almost the same as that of the rotation speed. As shown in Figure 6c, when the soil depth is less than 70 mm, the stone removal rate increases rapidly as the rotation speed increases. When the soil depth is more than 70 mm, the stone removal rate changes slightly as the rotation speed increases, and exhibits a downward trend. When the rotation speed is small, the stone removal rate increases rapidly as the soil depth increases; however, when the rotation speed increases, the changes in the stone removal rate decrease as the soil depth increases. Finally, the stone removal rate reaches the maximum and does not change even if the soil depth increases.

4.2.2. Stone Removal Efficiency

The forward speed, soil depth, rotation speed, and the interaction between the soil depth and rotation speed have significant influence on the stone removal efficiency. As shown in Figure 6d, with the increase in the soil depth, the stone removal efficiency gradually increases and finally does not change. With the increase in the rotation speed, the stone removal efficiency gradually decreases, and the amount of the reduction is small.

4.2.3. Operating Resistance

The forward speed, soil depth, and rotation speed, as well as the interactions between forward speed and soil depth, have significant influence on the operating resistance. As shown in Figure 6e, the operating resistance increases as the forward speed increases; however, the operating resistance increases more strongly as the soil depth increases. As shown in Figure 6f, the operating resistance increases as the soil depth increases. When the soil depth is less than 70 mm, the operating resistance gradually increases as the rotation speed increases; however, the increase is relatively gentle. When the soil depth is greater than 70 mm, the operating resistance gradually decreases as the rotation speed increases.

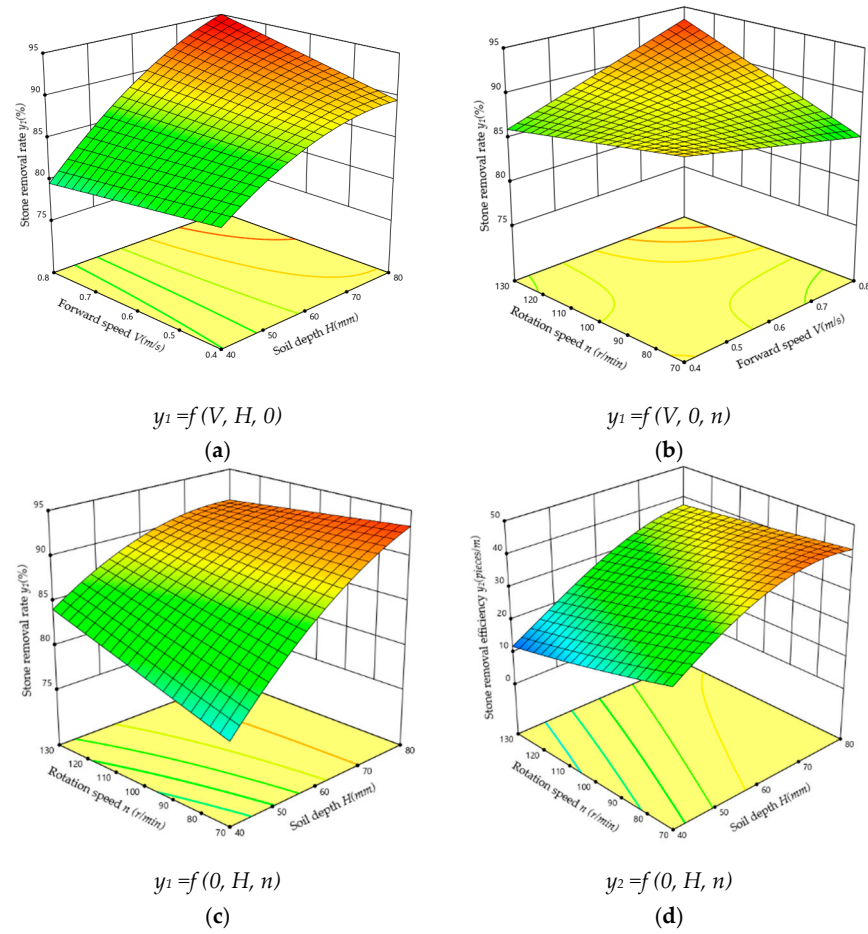


Figure 6. Cont.

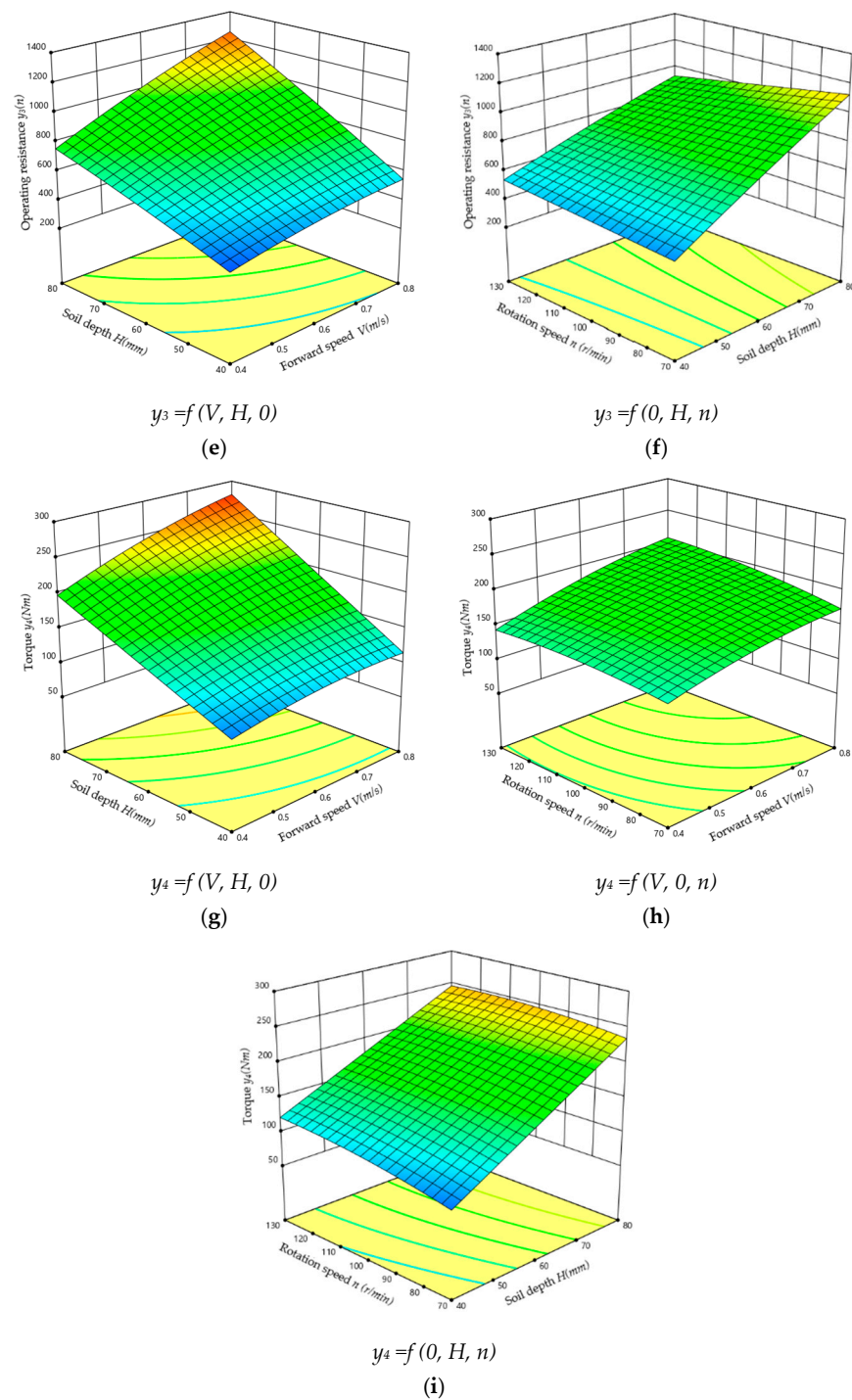


Figure 6. Response surfaces for interaction between factors: (a) effect of forward speed and soil depth on the stone removal rate; (b) effect of forward speed and rotation speed on the stone removal rate; (c) effect of soil depth and rotation speed on the stone removal rate; (d) effect of soil depth and rotation speed on the stone removal efficiency; (e) effect of forward speed and soil depth on the operating resistance; (f) effect of soil depth and rotation speed on the operating resistance; (g) effect of forward speed and soil depth on the torque; (h) effect of forward speed and rotation speed on the torque; and (i) effect of soil depth and rotation speed on the torque.

4.2.4. Torque

The forward speed, soil depth, and rotation speed, as well as the interactions among the three factors, have a significant influence on the torque. As shown in Figure 6g, the

torque increases as the forward speed and soil depth increase. As shown in Figure 6h, the increase in the forward and rotation speeds leads to a gentle increase in torque, and the two factors basically have the same trend of influence on the torque. As shown in Figure 6i, the rotation speed has little influence on the torque, and the torque gently increases as the rotation speed increases. When the rotation speed is approximately 100 r/min, the torque does not increase as the rotation speed increases. The soil depth has a great influence on the torque, and the torque increases rapidly as the soil depth increases.

4.3. Comprehensive Optimal Design

To rank the importance of the response values depending on the operation principle of “good, fast, and effortless”, and according to Equation (10), the optimal solution set was determined. To meet the requirements of the forward speed and operating speed ratio, the optimal solution is selected as forward speed $V = 0.5$ m/s, soil depth $H = 61.28$ mm, and rotation speed $N = 110.85$ r/min. The theoretical response values under the combination of parameters are stone removal rate $y_1 = 88.37\%$, stone removal efficiency $y_2 = 34.86$ pieces/m, operating resistance $y_3 = 692.66$ N, and torque $y_4 = 169.6$ Nm. The expected value that the optimal solution satisfies the optimization condition is 0.746. The optimal operating parameters were rounded to forward speed $V = 0.5$ m/s, soil depth $H = 61$ mm, and rotation speed $N = 110$ r/min, and the optimal operating parameters were used to perform the simulation experiment to verify the validity and usability of the equations and results. The simulation experiment results were the stone removal rate $y_1 = 85.65\%$, stone removal efficiency $y_2 = 35.47$ pieces/m, operating resistance $y_3 = 719.23$ N, and torque $y_4 = 174.89$ Nm, which were consistent with the theoretical results. Therefore, the equations and results were credible and could provide support for the field test. Figures 7 and 8 show the simulation experiment effect of the optimal operating parameters and motion trajectory of the stones.

$$\left\{ \begin{array}{l} \max y_1(V, H, n) \\ \max y_2(V, H, n) \\ \min y_3(V, H, n) \\ \min y_4(V, H, n) \\ \left\{ \begin{array}{l} v = 0.5 \text{ m/s} \\ 40 \leq H \leq 80 \\ 70 \leq n \leq 130 \end{array} \right. \end{array} \right. \quad (10)$$



Figure 7. Simulation experiment effect of the device: (a) primary distribution of stones and (b) stone distribution after processing.

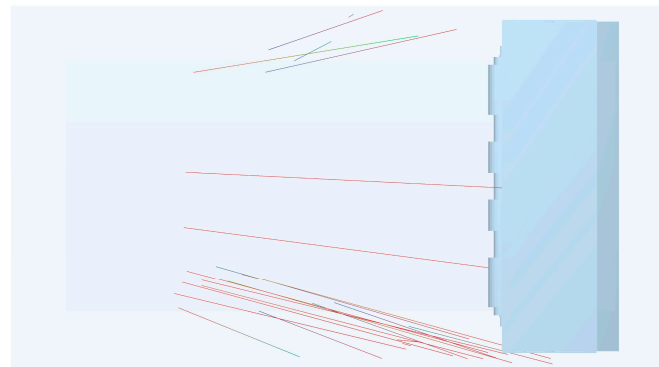


Figure 8. Motion trajectory of stone.

4.4. Comparisons with Field Measurements

4.4.1. Field Test Conditions and Method

Owing to the COVID-19 pandemic and the rainy weather, the field test using the proposed device was conducted at the research and teaching base of South China Agricultural University, located in Yuezhou Road, Tianhe District, Guangzhou City, Guangdong Province ($23^{\circ}10'13.8''$ N, $113^{\circ}22'28.2''$ E) on 31 December 2020. The experimental area was approximately 2000 m^2 , and the average soil moisture content and compaction were 20.81% (0–150 mm depth) and 198.5 kPa (0–100 mm depth), respectively. Two squares with the same area ($800 \times 800\text{ mm}$) were arranged 2000 mm apart in the operation area, and the number of stones in the two squares was 10 (sparse square) and 30 (dense square), respectively, which were dyed red and green, respectively, to facilitate stone picking up and data statistics, as shown in Figure 9a. The size of the stones in the two squares was randomly distributed in the range of 40–80 mm. The operating parameters of the device were set according to the optimal combination obtained from the simulation experiment. The field test was repeated six times, and the operating parameters of the device were calibrated before each operation to ensure the accuracy of the parameters, as shown in Figure 9b. The device was connected to the tractor (LOVOL M804-B wheeled tractor, Weifang, China) using a trifilar suspension system. Owing to the limitations of the experimental conditions, only the stone removal rate was counted, and the groove-forming effect was observed.



Figure 9. Preparation for the field test: (a) distribution of stone and (b) calibration of operation parameters.

4.4.2. Field Test Results

The field test results are shown in Table 8. The coefficient of variation of the stone removal rate of six repeated field tests was found to be 8.98%; therefore, the operating performance of the device was stable. The average stone removal rate of six repeated field tests was 77.23%, and the difference compared with the simulation experiment results

(85.65%) was less than 10%, which confirms the credibility of the simulation experiment results. In the six groups of field tests, the average stone removal rate of the two kinds of stone with different distribution densities were 82.78% and 71.67%, respectively. The stone removal rate in densely distributed areas were higher than those in less distributed areas. However, the difference between them was not significant, that is, the distribution density of the stones had no significant effect on the stone removal rate of the device. Figure 10 shows the field test site. The observation method was used to evaluate the groove-forming effect, and the comprehensive analysis showed that the effect reached the design requirements. Figure 11 shows the effect of groove forming and seedling growth.

Table 8. Field test results.

No	1		2		3		4		5		6	
Total stone	Dense square	Sparse square	Dense square	Sparse square	Dense square	Sparse square	Dense square	Sparse square	Dense square	Sparse square	Dense square	Sparse square
Number of stone removed	26	8	27	6	23	7	27	6	20	7	26	9
Stone removal rate (%)	86.67	80	90	60	76.67	70	90	60	66.67	70	86.67	90
Single stone removal rate (%)	83.34		75		73.33		75		68.34		88.34	
Average stone removal rate (%)	77.23											



(a)



(b)

Figure 10. Distribution and statistics of stones: (a) stone distribution after processing and (b) collection of stones.



Figure 11. Effect of groove formation and seedling growth.

5. Conclusions

In order to improve the quality of the seedbed, we proposed a seedbed clearing and shaping device for dry direct-seeded rice, which was developed using theoretical calculations, discrete element modelling simulations, and field tests. The device can be used to remove stones in the seeding area, break soil blocks, and form grooves without disturbing the deep soil. The research results showed that:

- (1) The primary and secondary factors that affect the stone removal rate (y_1), stone removal efficiency (y_2), operating resistance (y_3), and torque (y_4) of the device were: soil depth $H >$ forward speed $V >$ rotation speed n and soil depth $H >$ rotation speed $n >$ forward speed V . Furthermore, the optimization parameters combination of the device was: forward speed $V = 0.5$ m/s, soil depth $H = 61$ mm, and rotation speed $N = 110$ r/min, which obtained a stone removal rate of $y_1 = 85.65\%$, stone removal efficiency of $y_2 = 35.47$ pieces/m, operating resistance of $y_3 = 719.23$ N, and torque of $y_4 = 174.89$ Nm.
- (2) The field verification tests results indicated that the stone removal rate y_1 was 77.23% under the optimization parameters combination. The mean relative error of the simulated experiments value was 8.42%, thereby indicating that the accuracy and effectiveness of the simulation model and regression equation and the good effect of the groove formation and seedling growth were obtained.

The field test of the proposed device successfully performed the removal of stones in the seedbed and the formation of the seeding furrow, thereby providing a high-quality seedbed for sowing and rice growth. In the future, subsequent trials of the device in other regions will be carried out to explore the adaptability of the machine to different working conditions and potential problems to optimize and improve the device.

Author Contributions: Methodology, H.L. and W.Y.; software, H.L. and L.F.; validation, W.Y.; formal analysis, H.L.; investigation, H.L. and L.F.; data curation, H.L.; writing—original draft preparation, H.L.; writing—review and editing, P.Y. and W.L.; visualization, H.L.; supervision, W.Y.; project administration, W.Y.; funding acquisition, W.Y. and H.L. All authors have read and agreed to the published version of the manuscript.

Funding: This research was funded by the National Key R&D Program (2021YFD2000405-4), Special Projects in Key Area of “Artificial Intelligence” of General Colleges and Universities in Guangdong Province (2019KZDZX1003), and Independent Research and Development Projects of Maoming Laboratory (2021ZZ001).

Institutional Review Board Statement: Not applicable.

Data Availability Statement: The data presented in this study are available on demand from the first author at lihui2021@hunaas.cn.

Acknowledgments: The authors would like to thank the teacher and supervisor for their technical support. Moreover, we would like to thank Hebei Zhengrong Agricultural Machinery Manufacturing Company for manufacturing the device. Additionally, we sincerely appreciate the work of the editor and the reviewers of the present paper.

Conflicts of Interest: The authors declare no conflict of interest.

References

1. Khush, G.S. Strategies for increasing the yield potential of cereals: Case of rice as an example. *Plant Breed.* **2013**, *132*, 433–436. [\[CrossRef\]](#)
2. Chen, S.; Cai, S.G.; Chen, X.; Zhang, G.P. Genotypic differences in growth and physiological responses of transplanting and direct seeding cultivation in rice. *Rice Sci.* **2009**, *16*, 143–150. [\[CrossRef\]](#)
3. Tuong, T.; Bouman, B. Rice production in water scarce environments. In *Water Productivity in Agriculture: Limits and Opportunities for Improvement*; Kijne, J., Barker, R., Molden, D., Eds.; CABI Publishing: Wallingford, UK, 2003; pp. 53–67.
4. Kakumanu, K.R.; Kaluvai, Y.R.; Nagothu, U.S.; Lati, N.R.; Kotapati, G.R.; Karanam, S. Building farm-level capacities in irrigation water management to adopt to climate change. *Irrig. Drain.* **2018**, *67*, 43–54. [\[CrossRef\]](#)

5. Tuong, T.P.; Castillo, E.G.; Cabangon, R.C.; Boling, A.; Singh, U. The drought response of lowland rice to crop establishment practices and N-fertilizer sources. *Field Crop. Res.* **2002**, *74*, 243–257. [\[CrossRef\]](#)
6. Liu, H.Y.; Hussain, S.; Peng, S.B.; Huang, J.L.; Cui, K.H.; Nie, L.X. Potentially toxic elements concentration in milled rice differ among various planting patterns. *Field Crop. Res.* **2014**, *168*, 19–26. [\[CrossRef\]](#)
7. Peng, S.B.; Tang, Q.Y.; Zou, Y.B. Current status and challenges of rice production in China. *Plant Prod. Sci.* **2009**, *12*, 3–8. [\[CrossRef\]](#)
8. Kumar, V.; Ladha, J.K. Direct Seeding of Rice: Recent Developments and Future Research Needs. *Adv. Agron.* **2011**, *111*, 297–413.
9. Farooq, M.; Siddique, K.H.M.; Rehman, H.; Aziz, T.; Lee, D.J.; Wahid, A. Rice direct seeding: Experiences, challenges and opportunities. *Soil Till. Res.* **2011**, *111*, 87–98. [\[CrossRef\]](#)
10. Singh, S.; Elamathi, S.; Ghosh, G.; Anandhi, P.; Masih, L.P. Performance of Direct-Seeded Rice as Influenced by Dual Cropping with Nitrogen Levels and Weed Management Practices in Prayagraj Region of Eastern Uttar Pradesh. *Natl. Acad. Sci. Lett.* **2020**, *43*, 399–402. [\[CrossRef\]](#)
11. Sandhu, N.; Subedi, S.R.; Singh, V.K.; Sinha, P.; Kumar, S.; Singh, S.P.; Ghimire, S.K.; Pandey, M.; Yadaw, R.B.; Varshney, R.K.; et al. Deciphering the genetic basis of root morphology, nutrient uptake, yield, and yield-related traits in rice under dry direct-seeded cultivation systems. *Sci. Rep.* **2019**, *9*, 9334. [\[CrossRef\]](#)
12. Kakumanu, K.R.; Kotapati, G.R.; Nagothu, U.S.; Kuppanan, P.; Kallam, S.R. Adaptation to climate change and variability: A case of direct seeded rice in Andhra Pradesh, India. *J. Water Clim. Chang.* **2019**, *10*, 419–430. [\[CrossRef\]](#)
13. Huang, M.; Zou, Y.B.; Jiang, P.; Xia, B.; Feng, Y.H.; Cheng, Z.W.; Mo, Y.L. Yield component differences between direct-seeded and transplanted super hybrid rice. *Plant Prod. Sci.* **2011**, *14*, 331–338. [\[CrossRef\]](#)
14. Liu, H.Y.; Hussain, S.; Zheng, M.M.; Peng, S.B.; Huang, J.L.; Cui, K.H.; Nie, L.X. Dry direct-seeded rice as an alternative to transplanted-flooded rice in Central China. *Agron. Sustain. Dev.* **2015**, *35*, 285–294. [\[CrossRef\]](#)
15. Xu, L.; Li, X.X.; Wang, X.Y.; Xiong, D.L.; Wang, F. Comparing the Grain Yields of Direct-Seeded and Transplanted Rice: A Meta-Analysis. *Agronomy* **2019**, *9*, 767. [\[CrossRef\]](#)
16. Anjum, S.A.; Tanveer, M.; Akbar, N.; Ashraf, U.; Ali, I.; Zohaib, A.; Manzoor, N. Comparative Efficacy of Various Weed Control Measures in Weed Dynamics, Yield and Profitability of Direct Seeded Fine Rice. *Pak. J. Agri. Sci.* **2017**, *54*, 129–134.
17. Singh, M.; Bhullar, M.S.; Chauhan, B.S. Influence of tillage, cover cropping, and herbicides on weeds and productivity of dry direct-seeded rice. *Soil Till. Res.* **2015**, *147*, 39–49. [\[CrossRef\]](#)
18. Muhammad, S.; Muhammad, I.; Sajid, A.; Muhammad, L.; Maqshoof, A.; Nadeem, A. The Effect of Different Weed Management Strategies on the Growth and Yield of Direct-Seeded Dry Rice (*Oryza sativa*). *Planta Daninha* **2016**, *34*, 57–64. [\[CrossRef\]](#)
19. Yao, Z.S.; Zheng, X.H.; Liu, C.Y.; Lin, S.; Zuo, Q.; Butterbach-Bahl, K. Improving rice production sustainability by reducing water demand and greenhouse gas emissions with biodegradable films. *Sci. Rep.* **2017**, *7*, 39855. [\[CrossRef\]](#) [\[PubMed\]](#)
20. Jabran, K.; Ullah, E.; Hussain, M.; Farooq, M.; Zaman, U.; Yaseen, M.; Chauhan, B.S. Mulching Improves Water Productivity, Yield and Quality of Fine Rice under Water-saving Rice Production Systems. *J. Agron. Crop Sci.* **2015**, *201*, 389–400. [\[CrossRef\]](#)
21. Hakansson, I.; Arvidsson, J.; Etana, A.; Rydberg, T.; Keller, T. Effects of seedbed properties on crop emergence. 6. Requirements of crops with small seeds. *Acta Agric. Scand. Sect. B—Soil Plant Sci.* **2013**, *63*, 554–563. [\[CrossRef\]](#)
22. Constantin, J.; Dürr, C.; Tribouillois, H.; Justes, E. Catch crop emergence success depends on weather and soil seedbed conditions in interaction with sowing date: A simulation study using the simple emergence model. *Field Crops Res.* **2015**, *176*, 22–33. [\[CrossRef\]](#)
23. Shi, L.R.; Zhao, W.Y.; Sun, W. Parameter calibration of soil particles contact model of farmland soil in northwest arid region based on discrete element method. *Trans. Chin. Soc. Agric. Eng.* **2017**, *33*, 181–187.
24. Dai, F.; Song, X.F.; Zhao, W.Y.; Zhang, F.W.; Ma, H.J.; Ma, M.Y. Simulative Calibration on Contact Parameters of Discrete Elements for Covering Soil on Whole Plastic Film Mulching on Double Ridges. *Trans. Chin. Soc. Agric. Eng.* **2020**, *50*, 49–56, 77.
25. Shi, Y.Y.; Sun, X.; Wang, X.C.; Hu, Z.C.; Newman, D.; Ding, W.M. Numerical simulation and field tests of minimum-tillage planter with straw smashing and strip laying based on EDEM software. *Comput. Electron. Agric.* **2019**, *166*, 105021. [\[CrossRef\]](#)
26. Hao, J.J.; Long, S.F.; Li, J.C.; Ma, Z.K.; Zhao, X.S.; Zhao, J.G.; Li, H. Effect of granular ruler in discrete element model of sandy loam fluidity in Ma yam planting field. *Trans. Chin. Soc. Agric. Eng.* **2020**, *36*, 56–64.
27. Barr, J.; Desbiolles, J.; Ucgul, M.; Fielke, J.M. Bentleg furrow opener performance analysis using the discrete element method. *Biosyst. Eng.* **2020**, *189*, 99–115. [\[CrossRef\]](#)
28. Yuan, J.; Li, J.G.; Zou, L.L.; Liu, X.M. Optimal Design of Spinach Root-cutting Shovel Based on Discrete Element Method. *Trans. Chin. Soc. Agric. Eng.* **2020**, *51*, 85–98.
29. Chen, Y.; Qin, Z.Y.; Rong, X.F. Study on Material's Breakage Behavior in a Jaw Crusher Based on EDEM. *Mach. Des. Manuf.* **2017**, *2*, 46–49.
30. Xing, J.J.; Zhang, R.; Wu, P.; Zhang, X.R.; Dong, X.H.; Chen, Y.; Ru, S.F. Parameter calibration of discrete element simulation model for latosol particles in hot areas of Hainan Province. *Trans. Chin. Soc. Agric. Eng.* **2020**, *5*, 158–166.